

Article

On the Fatigue Strength of Welded High-Strength Steel Joints in the As-Welded, Post-Weld-Treated and Repaired Conditions in a Typical Ship Structural Detail

Antti Ahola ^{1,*}, Kalle Lipiäinen ¹, Juuso Lindroos ², Matti Koskimäki ¹, Kari Laukia ² and Timo Björk ¹¹ Laboratory of Steel Structures, LUT University, Yliopistonkatu 34, FI-53850 Lappeenranta, Finland² Aker Arctic Technology Oy, Merenkulkijankatu 6, FI-00980 Helsinki, Finland

* Correspondence: antti.ahola@lut.fi; Tel.: +358-50-475-2825

Abstract: Weld quality and life extension methods of welded details in ship structures made of high-strength and ultra-high-strength steels are of high importance to overcome the issues related to the fatigue characteristics of welded high-strength steels. The current work experimentally and numerically investigated the fatigue strength of a longitudinal stiffener detail, typically present in the bulkhead connections of ship hull. Two high-strength steel grades, namely EQ47TM and EQ70QT steels, were studied in welded plate connections using gas metal arc welding with rutile-cored wires. Fatigue tests were carried out on both small-scale specimens under axial and large-scale beam specimens under four-point bending loading. In addition to the joints tested in the as-welded condition, the high-frequency mechanical impact (HFMI) treatment was considered as a post-weld treatment technique in the fatigue test series. Furthermore, the large-scale beam specimens were pre-fatigued until substantial fatigue cracks were observed, after which they were re-tested after weld repairing and post-weld treatments to investigate the potential to rehabilitate fatigue-cracked ship details. The joints in the as-welded condition were performed in accordance with the current design recommendations. Due to the severe transition from the base material to the weld reinforcement in the joints welded with the rutile-cored wire, a successful HFMI treatment required geometrical modification of weld toe using a rotary burr to avoid any detrimental sub-cracks at the HFMI-treated region. Alternatively, the use of solid filler wires could potentially overcome these issues related to the welding quality. Repaired and post-weld-treated welds performed well in the re-tests, and the fatigue strength was almost twice higher than that of tests in the as-welded condition.

Keywords: fatigue; welded joint; ship structure; post-weld treatment; weld repair; high-strength steel

Citation: Ahola, A.; Lipiäinen, K.; Lindroos, J.; Koskimäki, M.; Laukia, K.; Björk, T. On the Fatigue Strength of Welded High-Strength Steel Joints in the As-Welded, Post-Weld-Treated and Repaired Conditions in a Typical Ship Structural Detail. *J. Mar. Sci. Eng.* **2023**, *11*, 644. <https://doi.org/10.3390/jmse11030644>

Academic Editor: Vincenzo Crupi

Received: 17 February 2023

Revised: 14 March 2023

Accepted: 16 March 2023

Published: 19 March 2023



Copyright: © 2023 by the authors. Licensee MDPI, Basel, Switzerland. This article is an open access article distributed under the terms and conditions of the Creative Commons Attribution (CC BY) license (<https://creativecommons.org/licenses/by/4.0/>).

1. Introduction

Fatigue is a decisive design criterion in ship and offshore structures to reach structural integrity and safety, as well as desirable lifecycle under cyclic load conditions. Of the structural elements, welded connections are usually susceptible to the fatigue failures due to their structural discontinuities, imperfections and misalignments [1–5], notch effects [6,7], high tensile residual stresses [8,9], and potential initial defects and flaws due to the welding [10,11]. Regarding the usage of advanced high-strength steel (HSS) materials, ship and offshore industries usually retained a certain level of conservatism but recent developments towards green technologies, as well as their potential regarding structural performance, led to an increasing interest in the applications of high-strength steels [12]. This particularly highlights the importance to consider the fatigue strength capacity of welded joints since, by default, an increase in the material strength does not contribute to an enhanced fatigue performance. High fatigue strength can be achieved by high-

quality welds via the enhanced welding process preparation [13] and/or post-weld treatments [14].

In the case of occurring fatigue cracks, repair welding provides a solution to extend the service life of structural elements. Schubnell et al. [15] showed that the fatigue strength of repair-welded high-strength and low-strength repair-welded joints was similar or higher than that of the joints in the as-welded (AW) condition. Even though it was proven that PWT techniques are able to extend fatigue life of cracked or pre-fatigued welded components, they are usually limited to the small crack sizes [16,17]. Consequently, their applications in engineering structures, such as large ships with multiple critical details, are still limited without having continuous monitoring of potential cracks. Many experimental studies tended to focus on the repair welding of small-scale (laboratory) specimens and there is still a lack of experimental evidence of the applicability of repair welding in large-scale components.

The objective of this study was to demonstrate the potential and limitations of PWTs and repair welding to enhance fatigue strength of high-strength ship steels welded with the shipyard procedures. As a result, the fatigue design methodologies and best practices can be established and developed for welded high-strength steel structures. Within this scope, the present study investigated the fatigue strength of welded high-strength and extra-high-strength ship structural steel grades, namely EQ47TM and EQ70QT. Experimental fatigue tests were carried out on the small-scale tensile specimens and large-scale beam specimens with the longitudinal bulkhead stiffener joint. The specimens were investigated in the AW, HFMI-treated and repair-welded conditions. Numerical finite element (FE) analyses were conducted to study stress concentrations at the structural and notch levels.

2. Materials and Methods

2.1. Materials

Two different high-strength ship structural steels, EQ47TM and EQ70QT grades, were selected for the experimental study. EQ47TM is currently used in some ship constructions, e.g., in container ships, and it was selected as a reference grade since it is the highest strength grade that does not require any case-by-case actions from the classification societies when used in container ship structures. EQ70QT is a 690 MPa class extra-high-strength steel delivered in the quenched and tempered for ship and offshore applications. The EQ70QT steel became available for ship building due to the increased production capacity. Strength-matching positional rutile-cored wires ($\phi 1.2$ mm): ESAB OK Tubrod 15.17 (T 46 3 1Ni P C1 2 H5) and ESAB OK Dual Shield 69 (T 69 6 Z P M21 2 H5) were used as filler metals for EQ47TM and 690QT steels, respectively, EN ISO 17632-A. Tables 1 and 2 presents the mechanical properties and chemical compositions of the studied materials, respectively.

Table 1. Mechanical properties of the studied materials. f_y is the yield strength of material, f_u is the ultimate strength of material, A is the elongation, and KV is the impact toughness (longitudinal, at plate top) at given temperature.

Material ID	Type	f_y (MPa)	f_u (MPa)	A (%)	KV at -40 °C (J)
EQ47TM	Nominal	460	570–720	17	46
	Mat. certificates	495–529	574–613	25–28	185
EQ70QT	Nominal	690	770–940	14	62
	Mat. certificates	841–855	874–879	16	195
OK Tubrod 15.17	Typical	544	613	26	124
Dual Shield 69	Typical	740	790	20	65
OK AristoRod 69 ^a	Typical	715	805	17	73

^a Only applied for the second set of the HFMI-treated joints.

Table 2. Chemical composition of the studied materials (wt-%).

Material ID	Type	C	Si	Mn	Cr	Mo	V	Ni	Cu
EQ47TM	Nominal	0.2	0.55	1.7	46	–	–	–	–
	Mat. certificate	0.098	0.42	1.56	0.05	0.003	0.012	0.44	0.011
EQ70QT	Nominal	0.2	0.55	1.7	46	–	–	–	–
	Mat. certificate	0.159	0.19	1.42	0.25	0.498	0.021	0.04	0.012
OK Tubrod 15.17	Typical ^a	0.05	0.34	1.15	–	–	–	0.96	–
Dual Shield 69	Typical ^a	0.095	0.34	1.25	–	0.4	–	2.8	–
OK AristoRod 69	Typical ^a	0.089	0.53	1.54	0.26	0.24	–	–	–

^aUndiluted weld metal.

2.2. Specimens and Welding Preparation

Two types of fatigue test specimens were fabricated: coupon-shape specimens for fatigue testing under the uniaxial tension load condition (Figure 1a), and large-scale welded beam specimens for fatigue testing under four-point bending. Henceforth, in this paper, these two specimen types are referred as tensile specimens and beam specimens as per the load configurations. The purpose for using beam specimens was to replicate the manufacturing conditions of such structural details and, on the other hand, achieve welding residual stress state comparable with actual large-scale structures. With the tensile specimens, the test frequency could be increased, and a higher number of specimens were tested. In total, 6 beam specimens and 21 tensile specimens were tested. In the tensile specimens, the bulkhead plate transverse to the beam (see Figure 1b) was not attached to the specimen during fatigue testing but was attached to the specimen during welding to replicate the accessibility at the cope hole detail.

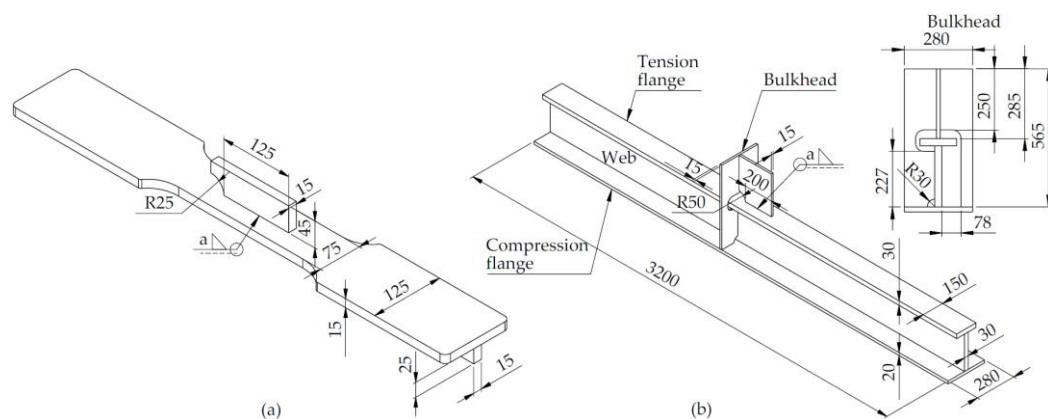
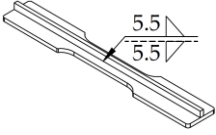
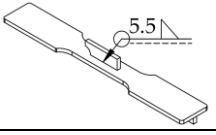


Figure 1. Shape and dimensions of the test specimens: (a) the tensile specimens, and (b) beam specimens (dimensions in mm).

The beam specimens were fabricated at shipyard with the normal welding procedure of the shipyard. The tensile specimens were fabricated in the laboratory conditions (at LUT University). First, the longitudinal fillet welds of the web-to-flange connections were welded with robotic welding. To compensate welding deformation due to the longitudinal seams and to have straight specimen for fatigue testing, pre-bending was applied in the welding of these welds. The fatigue-critical longitudinal gusset was welded with manual welding. Table 3 presents the welding parameters of the tensile specimens.

Table 3. Welding parameters of the tensile specimens. U is the welding voltage, I is the current, v_{travel} is the torch traveling speed, and v_{wire} is the wire feed rate.


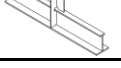
Weld Description	Pass ID	Pos.	U (V)	I (A)	v_{travel} (mm/s)	v_{wire} (m/min)
	1–2	PB	25.9	310–320	4	13.5
	1–2 ^a	PB	28	310–320	4	12.0

^a Welded with two passes with the start and stop positions at the gusset tips.

2.3. High-Frequency Mechanical Impact Treatment

In selected specimens, HFMI treatments were carried out using a commercial pneumatic HiFIT ‘Basic’ device [18] with a pin diameter of 4 mm. In the first set of the HFMI specimens (see Table 4, column ‘HFMI’), the HFMI treatment was carried without any pre-processing of weld toe. However, as shown by the results (see Section 3), the use of rutile-cored caused severe transition from the base metal to the weld metal. As a result, the HFMI treatment unsuccessfully processed the fatigue-critical weld toe, no improvement in the fatigue strength was necessary found. Due to these reasons, the weld toes in the second set of HFMI-treated specimens were burr-ground (rotary burr with diameter of 6 mm) before the HFMI treatment (see Table 4, column ‘BG+HFMI’). With the grinding, the transition was smoothened to enable accessibility to the toe position with the HFMI tool.

Table 4. Testing matrix. Detailed descriptions of the PWTs (burr grinding, BG, and HFMI treatment are given in Section 2.2).

Specimen Type	Material Grade	AW	HFMI	BG+HFMI	Repair-Welded
	Tensile	EQ47	4	2	–
		EQ70	4	4	7
	Beam	EQ47	2	1	–
		EQ70	2	1	–

2.4. Repair Welding of the Beam Specimens

In the beam specimens, the repair welding was also studied to investigate the potential to rehabilitate pre-fatigued structures. The repair welding was applied to those four specimens tested in the AW condition. The fatigue tests of the beam specimens were stopped after crack reaching a depth of 10–15 mm. This depth corresponds to the crack size that can be clearly seen observed in real applications but is still repairable. The repair welding procedure was conducted as follows (Figure 2):

1. Fatigue crack was removed by plasma arc gouging and rotary burr;
2. The gouged dent was inspected with the liquid penetrant to ensure that the whole crack was removed before starting repair welding process;
3. Tungsten inert gas (TIG) welding was applied to re-melt and re-shape the deepest point of the dent;
4. Multipass TIG welding with the consumable of ESAB OK Tigrod 13.09 (ø2.4 mm) and GMA welding with solid wire of ESAB OK 12.51 (for the EQ47 steel) and 13.29 (for the EQ70 steel) were used to fill the dent;
5. In the cope hole details, the weld reinforcement was ground to flush with a lamellar rotary grinder. At the opposite side of the gusset, HFMI treatment was applied.

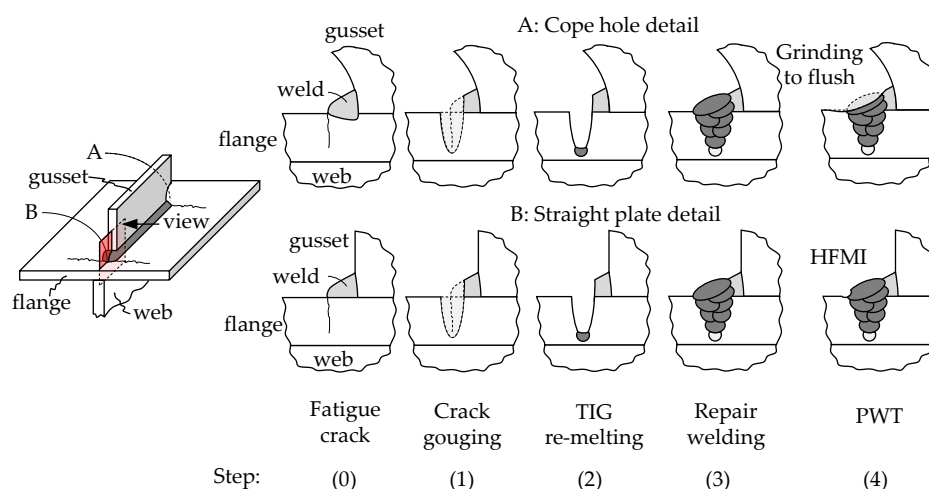


Figure 2. Schematic description of weld repair processing.

2.5. Residual Stress Measurements

Before the fatigue testing (see Section 2.5), welding-induced residual stresses were characterized in both tensile and beam specimens. The surface residual stresses, in the longitudinal loading direction of the specimens, were measured using an X-ray diffractometer (XRD, Stresstech X3000 G3) with a collimator spot diameter of 1 mm in the vicinity of the critical weld toes (see Figure 3). From the specimens in the AW condition, the residual stress distribution starting from the weld along the specimen was measured while in the HFMI-treated specimens, residual stresses were measured only from the HFMI groove.

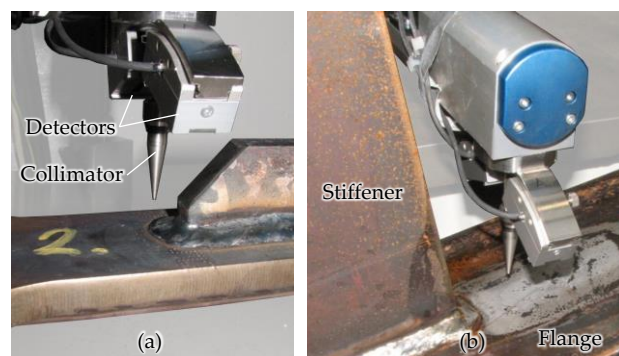


Figure 3. Residual stress measurements of (a) a tensile specimen and (b) beam specimen.

2.6. Fatigue Testing

Fatigue tests were carried out using two servo hydraulic fatigue test rigs. The tensile specimens were tested using uniaxial constant amplitude (CA) loading with the clamping system under applied stress ratios of $R = 0.1$ and $R = 0.5$ (Figure 4a). The beam specimens were fatigue-tested under CA four-point bending with a constant bending moment and zero shear force between the inner press rolls (Figure 4b). The distances between inner rolls and outer rolls were 700 mm and 3220 mm, respectively. The end criterion for fatigue testing in the tensile specimens was the total rupture of the specimen. As the beam specimens were pre-fatigued before the repair welding, the tests were stopped when substantial fatigue cracks were observed in the specimens—usually with the crack depth of $a = 10$ – 15 mm—enabling weld repairs in the flange. Subsequently, fatigue testing of these beam specimens was continued until cracks with substantial size in the flange were observed.

The test specimens were equipped with strain gages to capture both nominal strains (verifying test loads in the beam specimens) located far from the joint area and local

structural strains at the hot-spot distances. In the tensile specimens (with the narrow web member), the HS strain gages were located at the $0.4t$ and $1.0t$ distances from the weld toe (type 'a' HS location). In the beam specimens, strain gages were located at 4 mm, 8 mm, and 12 mm distances from the weld toes as per the type 'b' HS location [19]. The HS strain measurement was conducted using strain gage chains. The strain gage instrumentation is exemplified in Figure 4c.

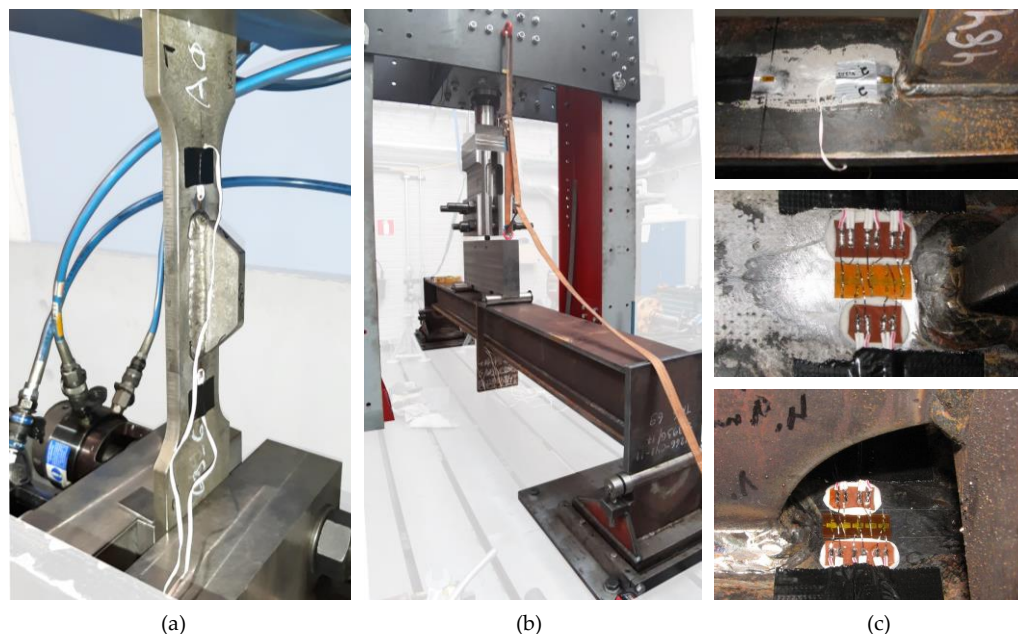


Figure 4. Fatigue testing equipment and instrumentation: fatigue tests of (a) the tensile specimens and (b) beam specimens, and (c) strain gage instrumentation.

2.7. Finite Element Analysis

To account for the effects of the studied specimen geometries and load configurations on the resulting stress concentrations, as well as to employ local approaches in fatigue assessments, numerical FE analyses were carried out using 8-noded brick shape linear solid elements with FEMAP 2022.2 (Siemens PLM) software. The geometry models for the tensile and beam specimens were created to include fictitious notch radii at the critical weld toes as per the concept of the effective notch stress (ENS) [20] with the reference radius of $r_{ref} = 1.0$ mm. Half symmetry was utilized in the model for the tensile specimens. At the critical toe position, element side length (tangential direction) was 0.10 mm with an aspect ratio of 2.5:1 (tangential/radial). The boundary and load conditions were modeled according to the test load conditions, i.e., under uniaxial tension and four-point bending loads in the tensile and beam specimens, respectively. Figure 5 presents the element mesh models together with the load and boundary conditions.

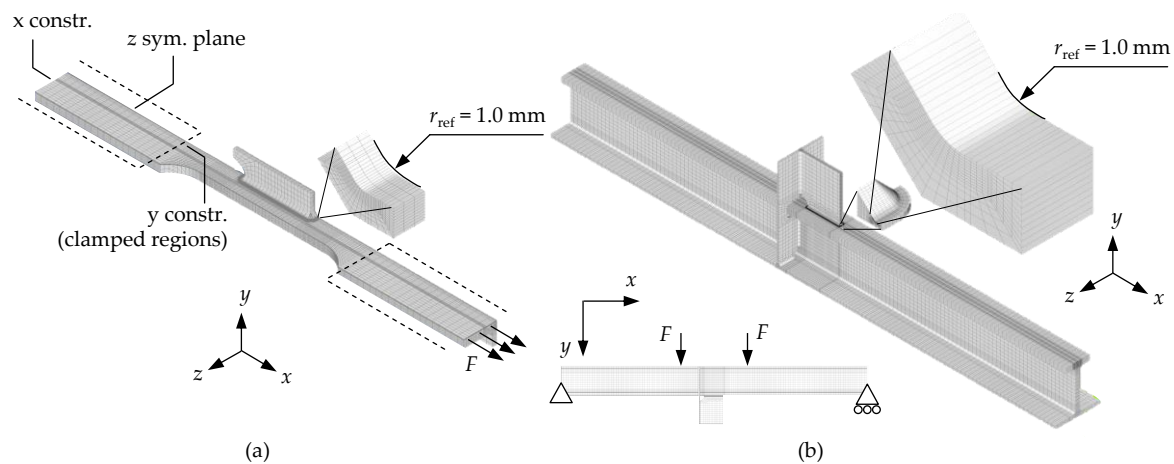


Figure 5. FE meshes for (a) the tensile specimens and (b) beam specimens (not in scale).

3. Results

3.1. Fatigue Tests

Figure 6 presents the results of the tensile specimens in the nominal stress system. The nominal stress refers to the value based on the axial load and cross-sectional area. For the longitudinal gusset length of 125 mm, FAT63/Class F1 (with a slope parameter of $m = 3$) can be selected as a characteristic design curve for joints in the AW condition [21–23]. For the HFMI-treated joints, FAT140 and FAT125 were recommended under the $R < 0.15$ load conditions for yield strengths of $550 \text{ MPa} \leq f_y < 750 \text{ MPa}$ and $355 \text{ MPa} \leq f_y < 550 \text{ MPa}$, respectively [24]. In this case, a slope parameter of $m = 5$ was applied. For $R = 0.5$, three FAT class decrease in fatigue strength was suggested [24]. Here, FAT100 and FAT90 can be claimed for these joints [24]. These FAT classes can be observed in Figure 6. In the AW condition, R ratio did not show distinguishing results; both load configurations were clearly above the design curve.

In the HFMI-treated conditions, the obtained fatigue strengths were highly related to the observed welding quality. The HFMI-treated EQ47 specimens suffered from the low welding quality, and no improvements were found compared to the AW specimens. The failure observations are presented in Section 3.2. In the EQ70 specimens, the HFMI treatments were more successful and even without BG processing, fatigue strengths above the FAT140 curve were obtained. With BG processing followed by the HFMI treatment (see BG+HFMI specimens in Figure 6), the successful HFMI treatment was confirmed but the fatigue strength of these specimens was comparable to the one of specimens without BG treatment. In the successful HFMI-treated specimens, with few exceptions, failures occurred either from the weld root or cut edge (see schematic presentations of failure modes in Figure 7). As the test results of these $R = 0.1$ HFMI specimens commensured into a single scatter band, an S - N curve was statistically fitted into these points, employing the conventional statistical approach [22]:

$$\log N_f = m \log \Delta \sigma + \log C \quad (1)$$

where N_f is the cycles to failure, m is the slope parameter, $\Delta \sigma$ is the stress range and C is the fatigue capacity. The mean curve, corresponding to the survival probability of $P_s = 50\%$, was fitted and the lower and upper bounds, and the characteristic ($P_s = 97.7\%$) curve was obtained as follows:

$$\log C_{97.7\%} = \log C_{50\%} - k \cdot \text{Std}v \quad (2)$$

where k is the characteristic value and $\text{Std}v$ is the standard deviation. With this approach, characteristic fatigue strength capacity of $\Delta \sigma_{c,97.7\%} = 163 \text{ MPa}$ was obtained for the EQ70 specimens in the HFMI-treated condition under the $R = 0.1$ load conditions (see Figure 6).

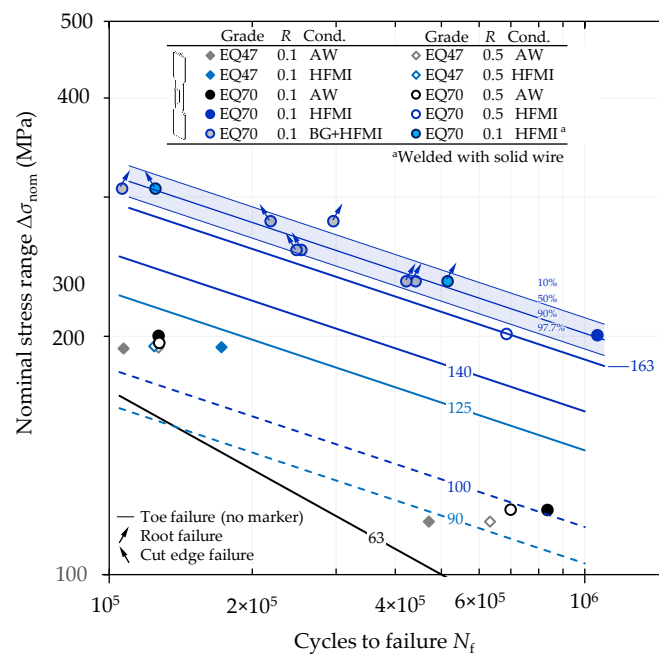


Figure 6. Fatigue test results of tensile specimens in the nominal stress system. BG+HFMI refers to the specimens welded specimens (rutile-cored wire) prepared by burr grinding followed by the HFMI treatment.

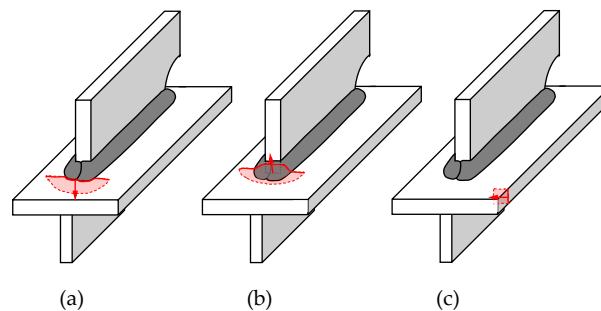


Figure 7. Observed failure locations in the specimens: from (a) weld toe, (b) weld root, and (c) thermally cut edge.

Figure 8 presents the fatigue test results for the beam specimens. For these specimens, the nominal stresses were obtained based on the acting bending moment and section modulus of the beam. The fatigue strength of the beam specimens was slightly lower than that of the tensile specimens. However, FAT63 was conservative in comparison to the test results.

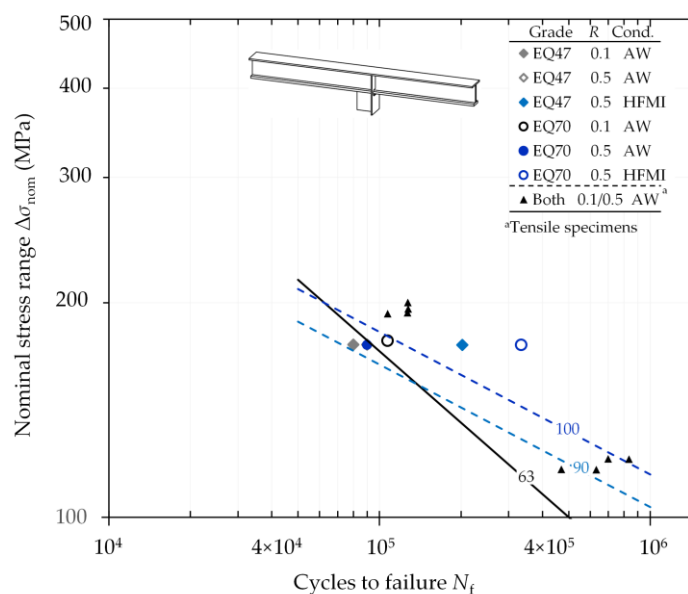


Figure 8. Fatigue test results of the beam specimens in the nominal stress system (^a Tensile specimens in Figure 5).

Figure 9 presents the fatigue test results of the repair-welded beam specimens in comparison to the tensile and beam specimens tested in the AW condition. The repair-welded specimens were also tested at the higher load levels to reach fatigue failures at similar number of cycles (close to 10^5 cycles) due to the lower test frequency. As can be seen, the repair-welded specimens performed better than the pre-fatigued specimens. Due to the PWTs, the failure mode changed from the weld toe failure to both weld root failure and toe failures from the HFMI-treated groove. In the S-N data plots of repair-welded specimens in Figure 9, the pre-fatigue test cycles were not accounted in the re-test; although, the weld root experienced the fatigue loading from the previous test. Considering these aspects, the fatigue lives would more clearly exceed the design lives of the corresponding design curves for the HFMI treatments.

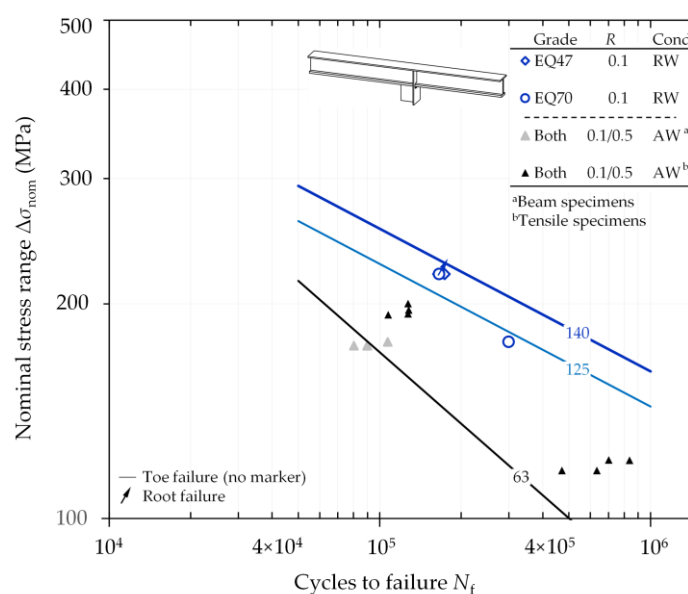


Figure 9. Fatigue test results of the repair-welded (RW) beam specimens in the nominal stress system (^a Beam specimens in Figure 7; ^b Tensile specimens in Figure 5).

3.2. Failure Observations

As mentioned in Section 3.1 (see also Figure 7), different failure modes were observed in the specimens. As expected, all specimens in the AW condition failed from the weld toe position; an exemplifying crack path was shown in Figure 10a. Those HFMI EQ47 specimens not reaching the design curve of FAT125 (see Figure 6) failed from the weld toe but outside the HFMI-treated groove, as demonstrated in Figure 10b. Figure 11a,b exemplified the weld toe and root failure modes, respectively, in the repair-welded specimens. The repair-welded regions were free of new fatigue cracks in all four studied specimens.

Figure 12a,b, respectively, demonstrates the failure modes in the successfully HFMI-treated prepared using rutile-cored wire (burr grinding and HFMI treatment) and solid wire (only HFMI treatment). The use of solid wire produced better pre-conditions for the HFMI treatment and failures occurred from the weld root. Similarly, burr grinding removed the material to enable accessibility to the original weld toe.

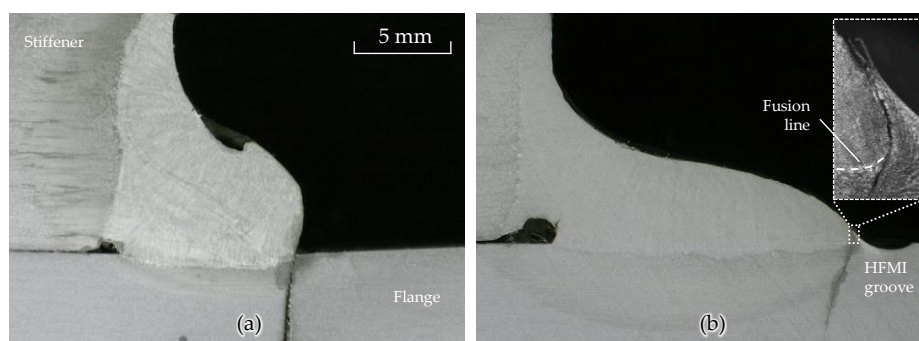


Figure 10. Macro graphs on the failures in the tensile specimens: (a) an EQ70 specimen failing from the weld toe, and (b) a HFMI-treated EQ47 specimen failing from the edge of the HFMI groove in the vicinity of the fusion line.

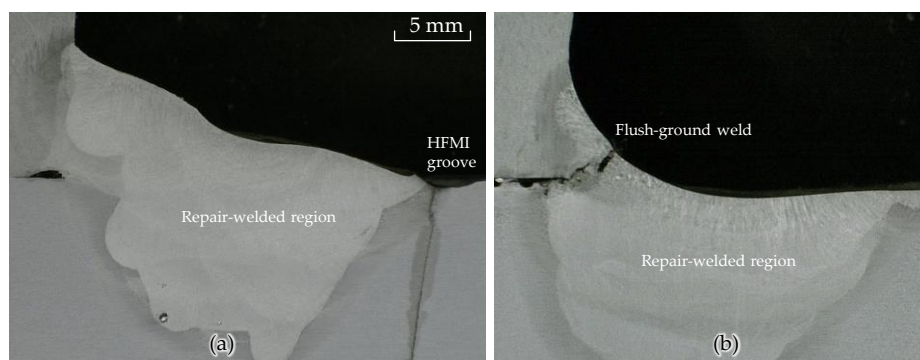


Figure 11. Macro graphs on the failures in the repair-welded beam specimens: (a) failure from the HFMI groove, and (b) failure from the weld root at the side of flush-ground toe (the cope hole side of the gusset).

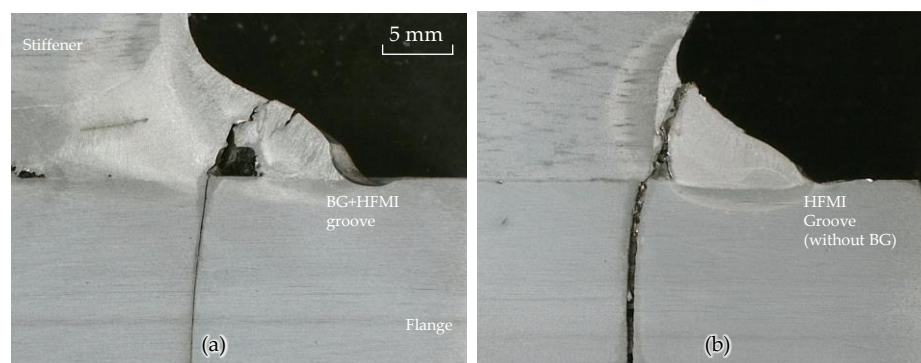


Figure 12. Macro graphs on the root failures in the successful HFMI treatments: (a) burr-ground and HFMI-treated specimen, and (b) HFMI-treated specimen (prepared using the solid wire).

3.3. Residual Stresses

Figure 13 presents the XRD measurement results on the surface residual stresses along the specimen's flange starting from the weld toe position. As expected, the welding residual stresses were highly in tension in both investigated specimen types in the AW condition—roughly 50% from the yield strength of the material. In the beam specimens, plate surface conditions potentially are a cause for the varying and highly scattering results, i.e., showing both tensile and compressive residual stress in the vicinity of the weld. However, the results provide an overview on the magnitude of the residual stresses in the specimens, confirming that the specimens represent real ship conditions with high tensile residual stresses. By applying the HFMI treatment, an introduction of compressive residual stresses was confirmed. Furthermore, a strain hardening phenomenon [25] could be identified by the measured full width at half maximum (FWHM) values, as seen in Table 5. The measurements were performed on the individual specimens of the series, and the bulkhead stiffener caused some geometrical inaccessibility to measure weld toe position (low tilting angles were applied in the XRD measurements). Due to these reasons, the results were slightly scattered, particularly in the case of the EQ47 specimens. In addition, compared to the yield strength of material, the EQ70 specimens had slightly lower residual stresses. Potentially, this can be explained by the microstructural (volume) changes at the heat-affected zone with the EQ70 steel with a higher carbon content.

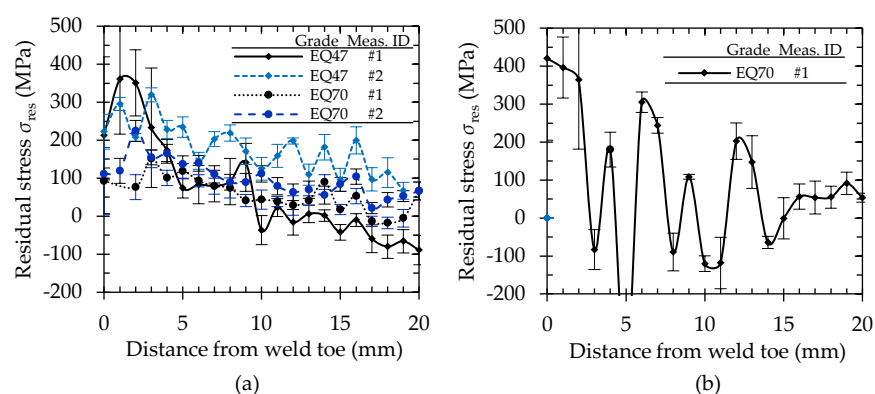


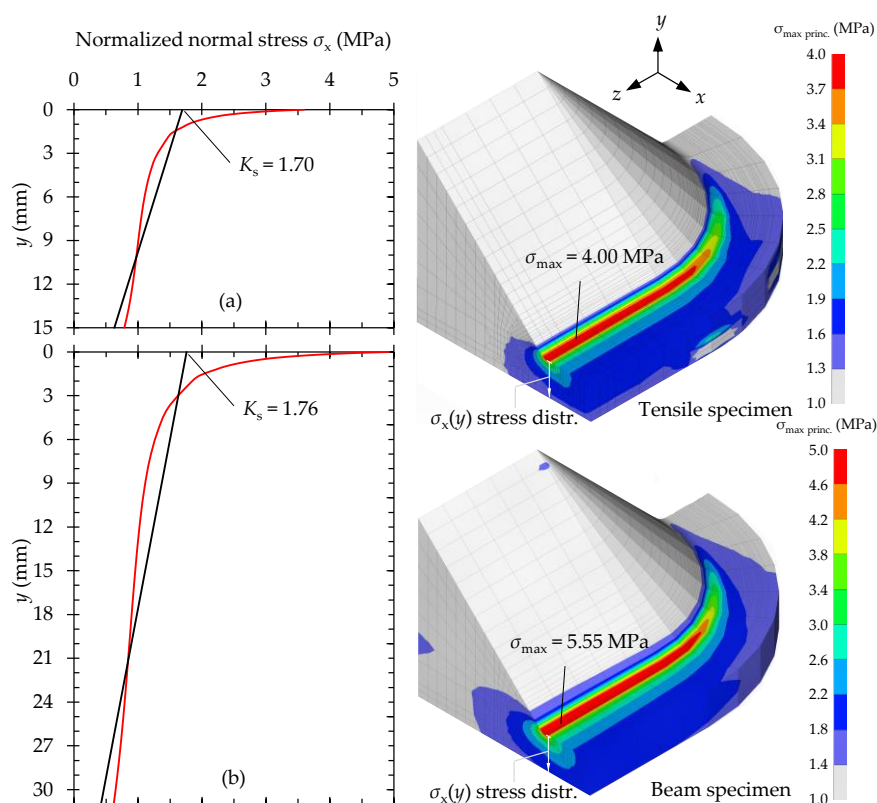
Figure 13. Residual stress measurement results in the specimens in the AW condition: (a) tensile specimens, and (b) beam specimen.

Table 5. Comparison of the measured residual stresses (at toe/groove position) and FWHM values in the AW and HFMI-treated tensile specimens.

Material Grade	σ_{res} (MPa)		FWHM (°)	
	AW	HFMI	AW	HFMI
EQ47	200...500	−200...−500	1.7...2.0	3.1...3.5
EQ70	70...130	−150...−350	2.2...2.5	3.5...4.2

3.4. Stress Concentrations and Fatigue Assessments Using Structural and Notch Stresses

Figure 14 presents the results of FE analyses in terms of the stress concentration factors (SCFs), obtained for the structural stress and ENS systems. By using the values shown in Figure 14, the fatigue notch factors of $K_t = 3.16$ ($= 5.55/1.76$) and $K_t = 2.27$ ($= 4.00/1.70$) were obtained for the beam and tensile specimens, respectively. These observations showed that the specimen type influenced the resulting SCF in both structural and notch stress levels. By employing these values, Figure 15 presents the S - N curves plotted using the local approaches. Repair-welded specimens were excluded from this evaluation. FAT100 for the structural HS stress approach and FAT225 for the ENS system (maximum principal stress criterion with $r_{\text{ref}} = 1.0$ mm) are the characteristic design curves (a slope parameter of $m = 3$). For the mean fatigue strength of butt-welded specimens in the ENS system, Nykänen and Björk [26] obtained 309 MPa. This is in line with the recommended safety factor of $j_\sigma = 1.37$ [27] and FAT225, giving 1.37×225 MPa = 308 MPa. For the HFMI-treated joints, FAT200 and FAT180 ($m = 5$) were suggested for yield strength of $550 \text{ MPa} \leq f_y < 750 \text{ MPa}$ and $550 \text{ MPa} \leq f_y < 750 \text{ MPa}$, respectively. For the ENS system, similar classes are FAT400 and FAT360 ($m = 5$) [24]. Compared to the nominal stress results (see Figures 6 and 8), the local approaches produced more conservative results. In addition, with the ENS system, the tensile and beam specimens seemingly fit better into a single scatter band. Compared to the mean fatigue strength obtained in the previous study [26], the results fit to these reasonably well and the ENS system produced conservative assessments.

**Figure 14.** Results of FE analyses: stress distributions and obtained structural SCFs and ENSs at the toe positions using the maximum principal stress criterion: (a) the tensile and (b) beam specimens.

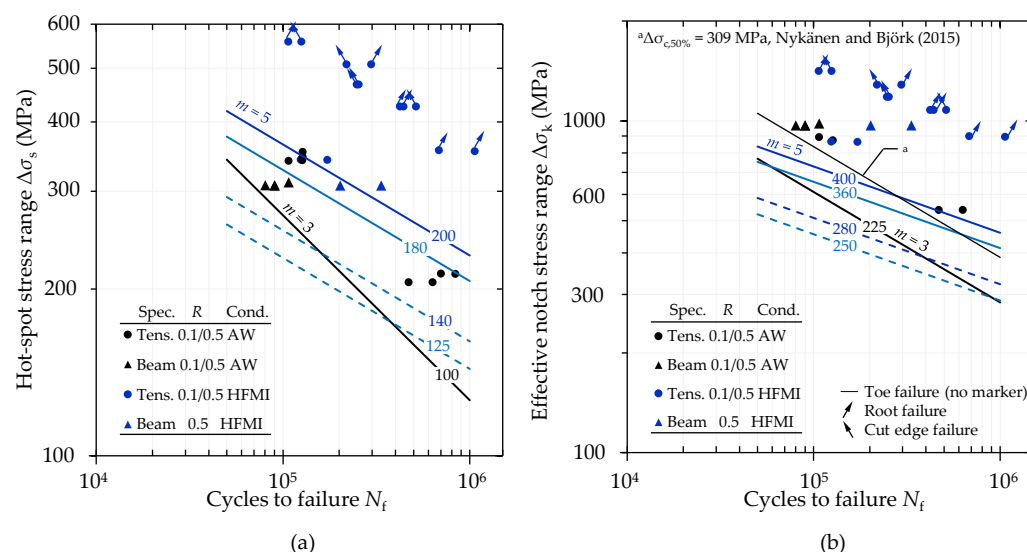


Figure 15. Fatigue test results in terms of (a) structural HS stress and (b) ENS systems. [26].

4. Discussion

The present study experimentally and numerically studied the fatigue strength of the welded bulkhead stiffener connection made of high-strength and extra-high-strength steels and susceptible to fatigue failures under cyclic loads. The fatigue test results (Figures 6 and 8) showed that, in the AW condition, the fatigue strength of these details were in line with the current recommendations. However, the number of tested AW specimens were limited, and an establishment of separate S - N curves would require more extensive testing. The produced welding quality, albeit not showing the optimal geometrical quality in the gusset tips, seemed to have sufficient fatigue strength. The beam specimens had slightly lower fatigue strength in the nominal stress system. The tensile specimens had lower plate thickness and shorter longitudinal stiffener than the beam specimens. Furthermore, the measured tensile residual stresses were slightly higher in the beam specimens than in the tensile specimens (Figure 13). However, the results showed the R ratio did not have a significant influence on the fatigue strength and, thus, the differences in the residual stresses cannot fully explain these differences. This is in line with the recommended practice [22] and experimental observations on the R ratio effects under different residual stress states [8]. In the beam specimens, the tests were interrupted after observing the crack, and thus, the obtained cycles to failure did not correspond to the total life, i.e., crack propagation life was not fully considered.

The initially fatigue-tested HFMI-treated specimens suffered from the sharp transition with low notch opening angle, and HFMI tool pin was inaccessible to treat the weld toe. The depth of the HFMI groove was acceptable and groove visually showed acceptable conditions; however, the pin did not reach the original toe position, as demonstrated by the crack paths. Based on the fatigue test observations on the HFMI-treated joints manufactured with the solid wire (Figures 6 and 7), the unmanufacturable HFMI treatment was related to the applied rutile-cored wires. These wires are specifically intended for all welding positions with good productivity, which is meaningful in shipyard conditions. However, from the HFMI treatment viewpoint, weld toe grinding, or other technique would be needed to confirm successful HFMI treatments. This was also outlined in the IIW Recommendations for the HFMI treatment [24]. In burr-ground and, subsequently, HFMI-treated specimens, two fatigue failure modes were observed: fatigue cracks originated from both weld root and cut edges. The change between these two failure modes is expectedly related to the weld root quality in the gusset tips. In the case of lack of fusion in the frontal surface of stiffener, this initial defect, transverse to the loading direction, acts

as a crack initiation/propagation location. If the successful fusion of the frontal surface is reached, a competing crack initiation from the cut edge is present.

The results of the successfully HFMI-treated joints showed conservative results with respect to the design curves (FAT140 with $m = 5$), with the characteristic fatigue strength of $\Delta\sigma_{c,97.7\%} = 163$ MPa, which indicates that HFMI treatment is a viable option to enhance fatigue strength of welded ship details made of (extra-)high-strength steels. The design recommendation for this detail category is FAT140 and, in the light of these results, one FAT class higher (FAT160) could be even suggested. In general, these findings are in line with the recent works conducted on the statistical re-evaluations of HFMI-treated joints made of high-strength steels [28]. The main focus of the HFMI experiments was on the EQ70 steel and further investigation would be needed for the 500 MPa class grades.

In the beam specimens, repair welding was applied after pre-fatiguing specimens resulting in an observable fatigue crack. After repair welding, the weld toes were post-weld-treated with the HFMI treatment and weld profiling (grinding to flush). With these procedures, the failures from the weld toe positions were avoided. The re-tested beam specimens failed from the weld root, instead, similar to some of those HFMI-treated tensile specimens. In fact, the fatigue strength capacity of these joints in the HFMI-treated condition is limited by the weld root fatigue capacity. To avoid such undesirable root failures, fully penetrating welds at the gusset tips should be used. From shipyard viewpoints, this would significantly increase workload related to the groove preparation. On the other hand, as failures were observed from the cut edges of flanges, it is evident that PWTs can enhance the fatigue strength of extra-high-strength steel weldments to the level of thermally cut edges, and thus, the full potential regarding the fatigue capacity of these steels can be claimed. The fatigue test results of those specimens failing from the cut edges were in line with the suggested fatigue class of FAT150 ($m = 3$) for thermally cut edges [29].

The structural SCFs were 1.70 and 1.76 for the tensile and beam specimens, respectively (Figure 14). Consequently, the structural HS stress method gave more conservative results than the nominal stress approach since SCFs were higher than the ratios FAT100/FAT71 (=1.41) and FAT100/FAT63 (=1.59). Moreover, the fatigue notch factors were different for the studied geometries, and an application of ENS commensured the data points into a same scatter band (Figure 15b). Since the weld geometry was similar in both tensile and beam specimens, the changes in the fatigue notch factors (K_t) can be explained by the thickness effect as well as, partially, by the stress gradient and increased share of bending stress in the nominally applied loading, which was identified as a key factor influencing notch SCFs in [30,31].

5. Conclusions

Based on the experimental and numerical work carried out within this work, the following conclusions can be drawn:

- Fatigue strength of welded bulkhead stiffener connection prepared with the rutile-coated wire was in line with the detail category of FAT63. The sharp transitions from the base metal to the weld reinforcement were observed, but based on the experimental results, sufficient fatigue strength was found.
- Pre-conditions for the successful HFMI treatment must be confirmed, either using burr grinding or equivalent geometry modifications, or employing solid filler wires. In this study, it was specifically related to the welding quality produced by the rutile-coated wires. With the successful treatment, the results were conservative compared to the design curves, and characteristic ($P_s = 97.7\%$) design fatigue capacity was 173 MPa at two million cycles. In the majority of the HFMI-treated specimens, failures occurred at the weld root or thermally cut edges and, consequently, it can be concluded that HFMI treatment is a viable option to enhance the fatigue performance of welded ship details made of extra-high-strength steels. If HFMI processes are

applied, careful attention should be paid on the weld root quality; the gusset end face should be welded without any lack of penetration.

- Repair welding can extend the fatigue life of structural components. In this study, the specimens experienced failures outside the repair-welded regions (mostly from the weld root), and fatigue lives were higher than that of pre-fatigued specimens. In repair welding, it is, thus, important to consider different failure modes from the different crack initiation points.
- With the investigated joint type, a use of the local approaches (structural HS stress method and ENS concept) produced more conservative results than the nominal stress method. Differences in the specimen geometries and load configuration gave different SCFs and can, thus, explain the differences found in the fatigue capacities when using the nominal stress system.

Author Contributions: Conceptualization, A.A. and M.K.; methodology, A.A. and T.B.; software, J.L. and A.A.; validation, M.K., A.A., and K.L. (Kalle Lipiäinen); formal analysis, M.K., A.A., and K.L. (Kalle Lipiäinen); investigation, A.A., K.L. (Kalle Lipiäinen), and M.K.; resources, M.K., A.A., and T.B.; data curation, M.K.; writing—original draft preparation, A.A.; writing—review and editing, A.A., K.L. (Kalle Lipiäinen), J.L., M.K., K.L. (Kari Laukia), and T.B.; visualization, A.A., K.L. (Kalle Lipiäinen); supervision, T.B. and K.L. (Kari Laukia); project administration, T.B. and K.L. (Kari Laukia); funding acquisition, T.B. and K.L. (Kari Laukia). All authors have read and agreed to the published version of the manuscript.

Funding: This research was funded by Business Finland in the Intelligent Steel Applications (ISA) project, grant number 7386/31/2018. The research work and manuscript were finished in the Fossil-Free Steel Applications (FOSSA) project funded by Business Finland (grant number 5498/31/2021). The APC was funded by LUT University.

Data Availability Statement: The research data are available upon request to the authors.

Acknowledgments: The authors wish to thank SSAB Europe Oy for providing the EQ steel materials for the experimental testing.

Conflicts of Interest: The authors declare no conflict of interest.

References

1. Björk, T.; Samuelsson, J.; Marquis, G. The Need for a Weld Quality System for Fatigue Loaded Structures. *Weld. World* **2008**, *52*, 34–46. <https://doi.org/10.1007/BF03266615>.
2. Eggert, L.; Fricke, W.; Paetzold, H. Fatigue Strength of Thin-Plated Block Joints with Typical Shipbuilding Imperfections. *Weld. World* **2012**, *56*, 119–128. <https://doi.org/10.1007/BF03321402>.
3. Lillemäe, I.; Lammi, H.; Molter, L.; Remes, H. Fatigue Strength of Welded Butt Joints in Thin and Slender Specimens. *Int. J. Fatigue* **2012**, *44*, 98–106. <https://doi.org/10.1016/j.ijfatigue.2012.05.009>.
4. Lotsberg, I. Stress Concentrations Due to Misalignment at Butt Welds in Plated Structures and at Girth Welds in Tubulars. *Int. J. Fatigue* **2009**, *31*, 1137–1345. <https://doi.org/10.1016/j.engfailanal.2016.11.006>.
5. Ahola, A.; Björk, T. Fatigue Strength of Misaligned Non-Load-Carrying Cruciform Joints Made of Ultra-High-Strength Steel. *J. Constr. Steel Res.* **2020**, *175*, 106334. <https://doi.org/10.1016/j.jcsr.2020.106334>.
6. Niraula, A.; Remes, H.; Lehto, P. Local Weld Geometry—Based Characterization of Fatigue Strength in Laser—MAG Hybrid Welded Joints. *Weld. World* **2023**. <https://doi.org/10.1007/s40194-023-01488-5>.
7. Braun, M.; Ahola, A.; Milaković, A.-S.; Ehlers, S. Comparison of Local Fatigue Assessment Methods for High-Quality Butt-Welded Joints Made of High-Strength Steel. *Forces Mech.* **2022**, *6*, 100056. <https://doi.org/10.1016/j.finmec.2021.100056>.
8. Baumgartner, J.; Bruder, T. Influence of Weld Geometry and Residual Stresses on the Fatigue Strength of Longitudinal Stiffeners. *Weld. World* **2013**, *57*, 841–855. <https://doi.org/10.1007/s40194-013-0078-7>.
9. Schroepfer, D.; Kromm, A.; Kannengiesser, T. Formation of Multi-Axial Welding Stresses Due to Material Behaviour during Fabrication of High-Strength Steel Components. *Weld. World* **2019**, *63*, 43–51. <https://doi.org/10.1007/s40194-018-0650-2>.
10. Jonsson, B.; Samuelsson, J.; Marquis, G. Development of Weld Quality Criteria Based on Fatigue Performance. *Weld. World* **2011**, *55*, 79–88. <https://doi.org/10.1007/BF03321545>.
11. Hobbacher, A.; Kassner, M. On Relation between Fatigue Properties of Welded Joints, Quality Criteria and Groups in Iso 5817. *Weld. World* **2012**, *56*, 153–169. <https://doi.org/10.1007/BF03321405>.
12. Billingham, J.; Sharp, J.V.; Spurrier, J.; Kilgallon, P.J. Review of the Performance of High Strength Steels Used Offshore. In *Health & Safety Executive, Research Report 105*; HSE Books: Norwich, UK, 2003.

13. Stoschka, M.; Leitner, M.; Posch, G.; Eichlseder, W. Effect of High-Strength Filler Metals on the Fatigue Behaviour of Butt Joints. *Weld. World* **2012**, *57*, 85–96. <https://doi.org/10.1007/s40194-012-0010-6>.
14. Haagenen, P.J. Fatigue Strength Improvement Methods. In *Fracture and Fatigue of Welded Joints and Structures*; MacDonald, K.A., Ed.; Woodhead Publishing: Cambridge, UK, 2011; pp. 297–329.
15. Schubnell, J.; Ladendorf, P.; Sarmast, A.; Farajian, M.; Knödel, P. Fatigue Performance of High- and Low-Strength Repaired Welded Steel Joints. *Metals* **2021**, *11*, 293.
16. Leitner, M.; Barsoum, Z.; Schäfers, F. Crack Propagation Analysis and Rehabilitation by HFMI of Pre-Fatigued Welded Structures. *Weld. World* **2016**, *60*, 581–592. <https://doi.org/10.1007/s40194-016-0316-x>.
17. Al-Karawi, H.; von Bock und Polach, R.U.F.; Al-Emrani, M. Fatigue Life Extension of Existing Welded Structures via High Frequency Mechanical Impact (HFMI) Treatment. *Eng. Struct.* **2021**, *239*, 112234. <https://doi.org/10.1016/j.engstruct.2021.112234>.
18. HiFIT The HiFIT Process. Available online: <https://www.hifit.de/en/> (accessed on 9 June 2022).
19. Niemi, E.; Fricke, W.; Maddox, S.J. *Structural Hot-Spot Stress Approach to Fatigue Analysis of Welded Components*, 2nd ed.; Springer Singapore: Singapore, 2017; ISBN 978-981-10-5567-6.
20. Fricke, W. *IIW Recommendations for the Fatigue Assessment of Welded Structures by Notch Stress Analysis*; Woodhead Publishing: Cambridge, UK, 2012.
21. EN 1993-1-9 Eurocode 3: Design of Steel Structures—Part 1–9: Fatigue; European Committee for Standardization: Brussels, Belgium, 2005.
22. Hobbacher, A. *Recommendations for Fatigue Design of Welded Joints and Components*; 2nd ed.; Springer International Publishing: Cham, Switzerland, 2016; ISBN 978-3-319-23757-2.
23. DNVGL-RP-C203 Fatigue Design of Offshore Steel Structures 2016. Available online: <http://www.dnvgl.com> (accessed 17 February 2023).
24. Marquis, G.B.; Barsoum, Z. *IIW Recommendations for the HFMI Treatment—For Improving the Fatigue Strength of Welded Joints*; Springer Singapore: Singapore, 2016; ISBN 978-981-10-2503-7.
25. Leitner, M.; Khurshid, M.; Barsoum, Z. Stability of High Frequency Mechanical Impact (HFMI) Post-Treatment Induced Residual Stress States under Cyclic Loading of Welded Steel Joints. *Eng. Struct.* **2017**, *143*, 589–602. <https://doi.org/10.1016/j.engstruct.2017.04.046>.
26. Nykänen, T.; Björk, T. Assessment of Fatigue Strength of Steel Butt-Welded Joints in as-Welded Condition—Alternative Approaches for Curve Fitting and Mean Stress Effect Analysis. *Mar. Struct.* **2015**, *44*, 288–310. <https://doi.org/10.1016/j.marstruc.2015.09.005>.
27. Radaj, D.; Sonsino, C.M.; Fricke, W. *Fatigue Assessment of Welded Joints by Local Approaches*; 2nd ed.; Woodhead Publishing: Cambridge, UK, 2006; ISBN 9781855739383.
28. Brunnhofer, P.; Buzzì, C.; Pertoll, T.; Rieger, M.; Leitner, M. Fatigue Design of Mild and High-Strength Steel Cruciform Joints in as-Welded and HFMI-Treated Condition by Nominal and Effective Notch Stress Approach. *Procedia Struct. Integr.* **2022**, *38*, 477–489. <https://doi.org/10.1016/j.prostr.2022.03.048>.
29. Lipiäinen, K.; Kaijalainen, A.; Ahola, A.; Björk, T. Fatigue Strength Assessment of Cut Edges Considering Material Strength and Cutting Quality. *Int. J. Fatigue* **2021**, *149*, 106263. <https://doi.org/10.1016/j.ijfatigue.2021.106263>.
30. Ahola, A.; Björk, T. Bending Effects on the Fatigue Strength of Non-Load-Carrying Transverse Attachment Joints Made of Ultra-High-Strength Steel. In Proceedings of the 8th International Conference on Structural Engineering, Mechanics and Computation (SEMC 2022), 5–7 September 2022, Cape Town, South Africa; pp. 1130–1135.
31. Ahola, A. Stress Components and Local Effects in the Fatigue Strength Assessment of Fillet Weld Joints Made of Ultra-High-Strength Steels. Ph.D. Thesis, LUT University, Lappeenranta, Finland. Available online: <http://urn.fi/URN:ISBN:978-952-335-595-8> (permanent address).

Disclaimer/Publisher’s Note: The statements, opinions and data contained in all publications are solely those of the individual author(s) and contributor(s) and not of MDPI and/or the editor(s). MDPI and/or the editor(s) disclaim responsibility for any injury to people or property resulting from any ideas, methods, instructions or products referred to in the content.